JOURNAL OF SPACECRAFT AND ROCKETS
Vol. 40, No. 2, March–April 2003

Laboratory Tests on 110-Volt Solar Arrays in Ion Thruster Plasma Environment

Mengu Cho,* Raju Ramasamy,† and Kazuhiro Toyoda‡
Kyushu Institute of Technology, Kitakyushu 804-8550, Japan
Yukishige Nozaki§
NEC Toshiba Space Systems, Ltd., Yokohama 224-8555, Japan
and
Masato Takahashi¶
National Space Development Agency, Ibaraki 305-8505, Japan

Ground-based experiments on the interaction between solar arrays of the Engineering Test Satellite VIII and ion thruster plasma are carried out. We carry out the experiments with two different designs of the solar arrays, and the results are compared. The electron current collection by the positively biased solar array is reported. The dependence of arcing rates on the bias voltage and the neutral gas density of negatively biased solar array are reported. Failure of the ion thruster neutralizer is simulated, and the sustained arc is observed at the gap between the adjacent cells of the solar array without room temperature vulcanization silicon grouting with the potential difference of 55 V and the current of 2.64 A. The grouting prevents a sustained arc even under the worst condition expected for the satellite. A sustained arc is observed bridging two interconnectors separated by 6 cm with an interstring voltage of 130 V and current of 2.64 A for the array with grouting.

Nomenclature

C	=	capacitance, F
C_{ext}	=	external capacitance, F
C_g	=	coverglass capacitance, F
E	=	energy, J
I	=	current, A
$I_{\max}$	=	maximum current flown between two strings via a power supply
n_e	=	electron density, m^{-3}
n_i	=	ion density, m^{-3}
n_n	=	neutral gas density, m^{-3}
n_0	=	charge exchange ion density at the source, m^{-3}
p	=	chamber pressure, torr
R	=	resistance, Ω
T_s	=	array temperature, K
V_a	=	inter-string bias voltage, V
V_b	=	array bias voltage, V
Δx	=	grid size in x direction, m
Δy	=	grid size in y direction, m
Δz	=	grid size in z direction, m
κT_e	=	electron temperature, eV
κT_i	=	in temperature, eV
ϕ_a	=	array potential, V

Subscripts

B	=	string B
e	=	electron
G	=	string G
i	=	ion
n	=	neutral
R	=	string R

Introduction

SINCE the end of the past decade, satellites in geosynchronous Earth orbit (GEO) have begun employing a bus voltage of 100 V to meet the demand for more power. At the same time, satellite size and longer operational lifetime requires a mass saving propulsion system, such as electric propulsion, which is now widely used especially for the north–south station keeping. In the past five years, the use of 100-V solar arrays has become widespread for GEO satellites because less plasma interaction is expected compared to low Earth orbit (LEO). The combination of the high-voltage solar array operating at a voltage of 100 V or higher and an electric propulsion system, however, raises concern over the issue of plasma interaction.

The National Space Development Agency of Japan plans to launch the Engineering Test Satellite VIII (ETS-VIII) in 2004. ETS-VIII is a 3-ton class geosynchronous satellite with a lifetime of 10 years. In ETS-VIII, new technologies such as high-voltage bus technology (110 V) and a large-scale deployable reflector of gold mesh are introduced to establish and verify the technology for future large-scale spacecraft systems. It has two 12-cm-diam Kaufman-type 20-mN xenon ion thruster systems. The thrusters are expected to operate twice a day for north–south station keeping. The time for each operation is 5 h, the operation is repeated five days a week, and it continues for 10 years. The solar array nearest to the ion thruster is approximately 5.2 m away in the direction approximately 41 deg from the center of the thrust beam. During the ion thruster operation, the plasma density around the array might reach as high as 10^{11} m^{-3} order of magnitude, which is much higher than GEO density ($\simeq 10^6$ m^{-3}) and is similar to the density of plasma in LEO. Detail of the estimate is given later. Hence, simulating the condition of GEO with ion thruster operation in a ground-based solar array testing will be similar to simulating the LEO plasma environment.

The ion thruster neutralizer will act as a plasma contactor, the solar array has a positive potential with respect to the plasma, and the spacecraft potential is nearly zero. The array with a positive

Received 19 March 2002; revision received 5 August 2002; accepted for publication 3 November 2002.

*Associate Professor, Department of Electrical Engineering, Tobata-ku; cho@ele.kyutech.ac.jp. Senior Member AIAA.

†Postdoctoral Fellow, Satellite Venture Business Laboratory; currently Postdoctoral Fellow, Department of Electronics, Tokai University, Hiratsuka 259-192, Japan.

‡Postdoctoral Fellow, Satellite Venture Business Laboratory, Tobata-ku; toyoda@ele.kyutech.ac.jp.

§Assistant Manager, Space Systems Department, Business Operation Division, Tsuzuki; nozaki.yukishige@ntspace.jp.

¶Associate Senior Engineer, Tsukuba; Takahashi.Masato@nasda.go.jp.

potential can undergo a phenomenon called snapover.[1] Snapover is a sudden and rather dramatic increase in the current collection by positive conductors that are surrounded by dielectric material. Having a positive potential above a certain value can lead to such a jump. Primary electrons in the plasma surrounding the solar arrays are accelerated toward the positively biased conductor. As the primary electrons strike the dielectric passing through the sheath above the array, one or more secondary electrons can be liberated. Many of these secondary electrons are collected by the conductor, causing the current to increase dramatically.[2,3] The gas-induced glow also occurs once the ionization occurs inside the sheath near the conductive surface. The ionization increases the positive charge inside the sheath, results in the increase of sheath thickness, and further increases the probability of the ionization collision inside the sheath.[4–6] This process leads to the anomalous ionization inside the sheath and results in a gas-induced glow.[3] This results in a substantial power losses for the spacecraft.

The increase of the electron current to the solar array from the surrounding plasma may drop the solar array potential. If the collected electron current exceeds the amount of current emitted by the neutralizer (0.5 ± 0.1 A for ETS-VIII), it is possible that the spacecraft potential will drop to a negative potential of -110 V, equal to the array output voltage. If the neutralizer fails to operate and cannot emit electrons, then the potential may drop to -1 kV, equal to the beam acceleration voltage. This potential drop leads to arcing. Arcing in a high-voltage solar array with a negative potential is mainly due to charging of the coverglass by ions from the surrounding plasma. Charging of the coverglass enhances the electric field at an interconnector, which is especially strong at the edges of the coverglass. The field enhancement at the triple junction where the coverglass, the interconnector, and the plasma meet leads to arcing.[7] Arcing results in an electromagnetic interference or surface deterioration. In most cases, an arc ends as a single pulse of discharge, which we call a trigger arc or simply refer as arc in the present paper. However, when certain conditions are met, a trigger arc may short circuit two points with different potentials over the solar array. The strings of the solar arrays are short circuited by the arc plasma. When the solar array power is sufficient to sustain the arc, the solar array circuit may provide continuous energy to the arc plasma.[8] We call such a state of arcing a sustained arc in the present paper. Once a sustained arc occurs, it may destroy the array circuit, causing the permanent loss of solar array power.

This is the second part of the report on the laboratory test of ETS-VIII solar arrays. In Ref. 9, the results of the charging experiment using a high-energy (greater than keloelectron volts) electron beam is reported. The purpose of the present paper is to verify that ETS-VIII arrays can function without any serious interaction with the ion thruster plasma. Because the density of the plasma used in this study is similar to a LEO environment, the results of the present study can be also applied to the study of 110-V arrays in LEO environment. Davis et al.[10] carried out tests on 100-V solar arrays to be used in LEO environment. In the present paper, we test two types of test coupons. One type has the gap between the solar array strings grouted by room temperature vulcanization (RTV) silicon rubber. This is the standard design implemented after the failure of the Tempo-2 satellite in 1997. The other type has no RTV grouting between the strings, which represents the design before 1997. We investigate how the presence of RTV grouting affects the nature of the interaction with the ion thruster plasma.

In the ground-based experiments, the full string of the solar array of one satellite cannot be tested. This allows us to insert additional capacitance into the external circuit to increase the energy release, and we examine whether that condition leads to a sustained arc. We increase the potential difference between the strings and determine the threshold for a sustained arc for the future use beyond ETS-VIII.

We describe the laboratory experiments, which simulate the interaction between the solar array and the ion thruster plasma. Then, we present the experimental results. In the experiment, first, we bias the test coupon positively to study the electron current collection. Second, we examine the conditions under which trigger arcs occur. We vary the bias voltage and the background gas density and measure the arcing rate and the current waveforms. Third, we examine the conditions for a sustained arc. We investigate the sustained arc between different solar array strings, that is, interstring sustained arc.[9] Finally, we conclude the paper.

Experiment

Plasma and Neutral Gas Densities Estimate Around Solar Array in GEO

The ion thruster beam consists of high-energy ion beams, neutralizer electrons, and charge exchange (CEX) ions. The laboratory diagnostic tests on the CEX plasma with a langmuir probe revealed that the CEX plasma density at 0.5 m from the thruster exit is between 2×10^{13} and 5×10^{13} m^{-3} (Ref. 11) The CEX plasma diffuses outward from the thruster plume due to the ambipolar diffusion. If we assume that the plasma diffuses radially and the density decrease is proportional to the inverse of square of the distance from the source, the density decreases by $(0.2/5)^2 = 0.0016$, where we assume that the source is a sphere of radius 0.2 m and the distance to the array is 5 m. Based on this estimate, we have chosen the plasma density in the range of 1×10^{11}–8×10^{11} m^{-3} for the experiment.

In orbital conditions, the neutral density near the solar array is estimated to increase to an order of magnitude of 10^{18} m^{-3}, approximately, at the extremely worst condition, where the solar array is at the downstream of the 22-N thruster (for east–west control). In our experiment, the neutral density is 10^{18}–10^{19} m^{-3}. The increase of the plasma and neutral densities will increase the risk of arcing on the solar array surface. Therefore, simulating the higher neutral and plasma densities in our experiments are regarded as the worst conditions, giving a safety margin to the array design.

Plasma Chamber

Figure 1 shows a schematic diagram of the experimental setup. The chamber is the same as the one used in Ref. 9. Xenon plasma is created using a Kaufman-type dc plasma source in the subchamber that generates the plasma temperature of 1.6 eV and density of 1×10^{11}–8×10^{11} m^{-3} at the neutral densities of 0.23×10^{19}–5.2×10^{19} m^{-3}. In one case, the plasma density along the axis of the chamber is varying between 7×10^{11} m^{-3} at 0.35 m from the gate valve and 5×10^{11} m^{-3} at 0.75 m from the gate valve. To simulate the operational temperature of 40°C at GEO, we use infrared lamps inside the chamber. The solar array is placed inside the chamber so that its face is parallel to the chamber axis. The 3-cm-diam aluminum langmuir probe is placed inside the chamber 0.4 m away from the array to study the plasma parameters inside the chamber during the experiments.

Solar Array Coupon

A detailed description of the ETS-VIII solar array is given in Ref. 9. Therefore, in this paper, we describe only the differences from Ref. 9. We use two different designs of solar array, one with RTV silicon rubber (W/RTV) between the strings and over the bus bars (Fig. 2b). The second is without RTV (W/O/RTV) between the

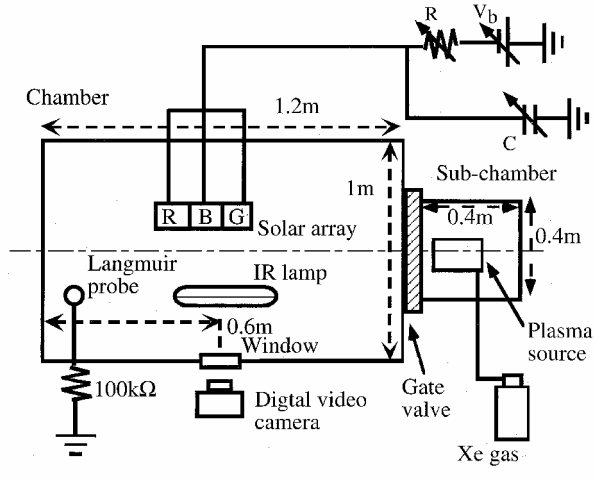

Fig. 1 Schematic of experimental setup.

Table 1 Experimental parameters

Case	Coupon type	V_b, V	C_{ext}, nF	n_n, 10^{19} m^{-3}	n_e, 10^{11} m^{-3}	V_a, V	I_{max}, A	p, 10^{-4} torr
1	W/RTV	+10–+370	NA	0.36–3.1	5–8	NA	NA	1.1–9.6
2	W/O/RTV	+10–+270	NA	0.28–3.1	1–3	NA	NA	0.87–9.6
3	W/RTV	−110–−600	NA	1.8	7–8	NA	NA	5.6
4	W/O/RTV	−700	NA	0.26–3.1	1–3	NA	NA	0.81–9.6
5	W/O/RTV	−500	200	2.2	1–3	10–55	2.64	6.8
6	W/RTV	−500	200	2.2	1–2	10–55	2.64	6.8
7	W/RTV	−500–−700	180–1440	1.6–2.1	2	55	2.64	5.0–6.5
8	W/RTV	−700	1440	1.8	2	60–130	2.64	5.6

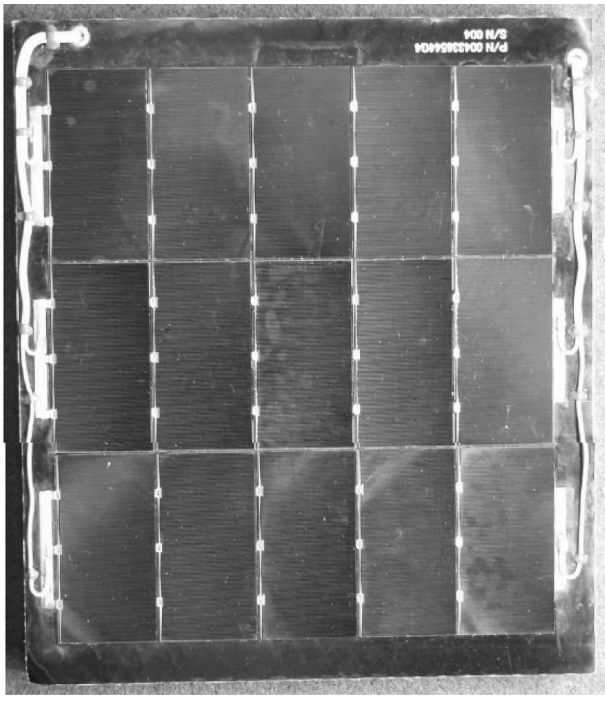

a) W/O/RTV

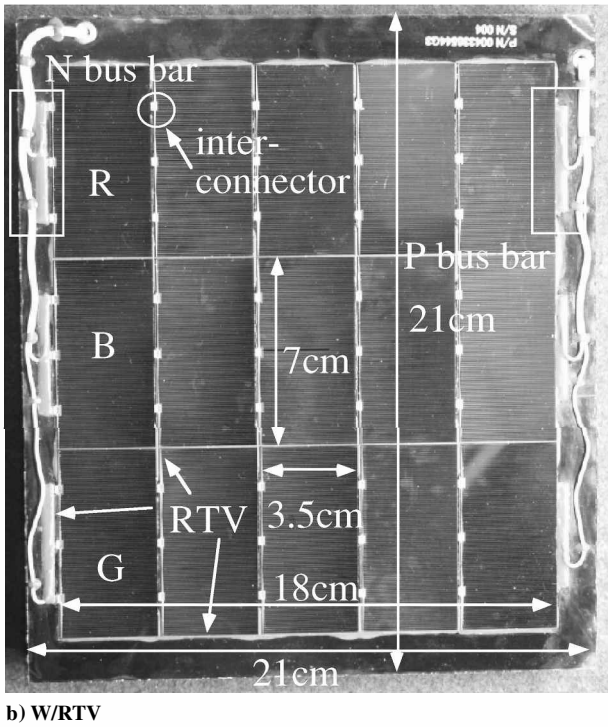

b) W/RTV

Fig. 2 Photographs of array coupons used in the experiment.

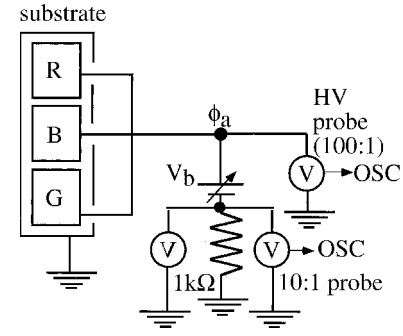

Fig. 3 Schematic of circuit configuration for cases 1 and 2.

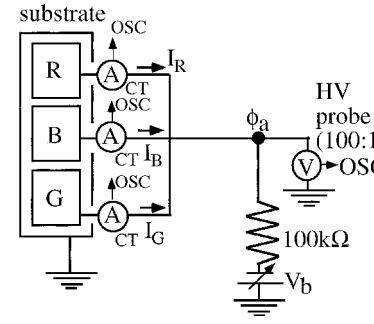

Fig. 4 Schematic of circuit configuration for cases 3 and 4.

cells (Fig. 2a). Whenever an array coupon is exposed to atmosphere, we bake it at a constant temperature of 70° ± 1°C for 2 h before we start an experiment. The array temperature during the experiment is kept at 40 ± 1°C.

Experimental Setup

We list the experimental parameters in Table. 1. The purpose of cases 1 and 2 is to study the snapover mechanism, measure the collected electron current, and identify the threshold voltage for the glow discharge. The circuit diagram is shown in Fig. 3. All three strings are positively biased at the same potential using the power supply, which is grounded through the 1-kΩ resistance. The collected current is measured as the voltage across the 1-kΩ resistance using a passive probe (10:1) and a digital multimeter. The array potential ϕ_a is monitored using a high-voltage (HV) probe. The HV probe and the passive probes are connected to a digital oscilloscope. The bias voltage is raised from a lower value to a higher. Each voltage is applied for about 1 min, and the collected current is read from the output of the multimeter before going to the next step. The oscilloscope is triggered manually when the gas-induced glow occurs at the solar array. The glow discharge is identified by looking at the video monitor with naked eyes.

The purpose of cases 3 and 4 is to study the trigger arc inception in relation to the bias voltage V_b and the neutral density n_n. During the measurements, all three strings (R, B, and G) of the solar array are biased to the same negative potential using a dc power supply in the external circuit, and whether an arc occurs at that condition is determined. The circuit diagram is shown in Fig. 4. The gas density

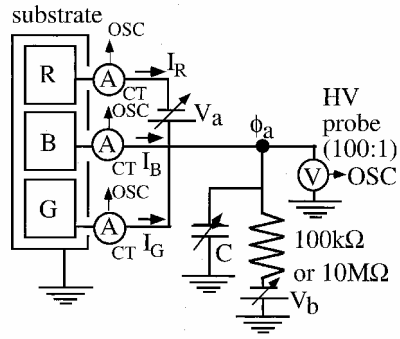

Fig. 5 Schematic of circuit configuration for cases 5–8.

is controlled by adjusting the xenon gas flow rate, and the pressure is measured by an ionization gauge. The temperature of the solar array is controlled by adjusting the power of infrared lamps and measured by using the thermocouple attached at the backside of the array coupon. The currents flowing through the strings, I_R, I_B, and I_G, are measured using current probes, and the array potential ϕ_a is monitored using an HV probe. The current probes and the HV probe are connected to the four-channel oscilloscope (Tektronix-TDS 224), which is triggered by the rise of the HV probe signal when an arc occurs at the array surface. A digital video camera is used to record the arc positions on the solar array during the experiment and to count the number of arcs. The video image is also used to infer the scale of arc from the intensity of the arc spot image.

The purpose of cases 5 and 6 is to measure the effect of V_a on the current waveforms of I_R, I_B, and I_G. The purpose of cases 7 and 8 is to find the threshold condition over which the sustained arc occurs for the W/RTV coupon. The circuit diagram for these cases is shown in Fig. 5. To simulate the potential difference between the adjacent strings, we apply the potential difference V_a between strings R and B using a floating dc power supply at the external circuit. The power supply operates as a constant power supply, but once the load suddenly collapses and the output is short circuited, the power supply operates as a constant current supply with a maximum current $I_{\max}$, which can be preset. The currents flowing through the strings, I_R, I_B, and I_G, are measured using current probes, and the array potential ϕ_a is monitored using an HV probe. Current probes and the HV probe are connected to the four-channel oscilloscope.

Results and Discussion

Electron Current Collection

Measured electron currents for W/RTV and W/O/RTV are given in Fig. 6. The collected current increases with the increase in the bias voltage for both the cases, and the increase is higher for W/O/RTV than W/RTV. In the measurement, we have increased the bias voltage from the lower value to the higher value. The neutral density is the same at $n_n = 1.8 \times 10^{19}$ m^{-3} for both cases. The plasma density is 7×10^{11} m^{-3} for W/RTV and 2×10^{11} m^{-3} for W/O/RTV. Although the plasma density for W/O/RTV is lower than W/RTV, the collected current by W/O/RTV is still higher than W/RTV. Higher electron current collection with W/O/RTV is due to that the area for the current collection is larger compared to W/RTV. In both designs, the probable sites for the electron collection are the interconnectors and the bus bars. In the case of W/O/RTV, the entire area of the bus bars (9.1 cm^2, approximately) is exposed in addition to the interconnector, whose total area is 5.4 cm^2, approximately. On the other hand, in the case of W/RTV, most of the bus bars are coated with RTV and less conductive area (mostly interconnectors) of the array is exposed to the plasma. From the results it is clear that coating the bus bars with RTV reduces the electron current collection.

In Fig. 6, the curve for W/RTV shows two jumps, at 160 and 220 V, which indicate snapover. As we increase the bias voltage further, the array surface shows a visible bluish glow. The glow appears over the conductive part of solar array when the positive bias voltage reaches the threshold voltage, which depends on the neutral density. Figure 7 shows an example of the current waveforms measured during the gas-induced glow discharges. In this example, the W/RTV coupon is

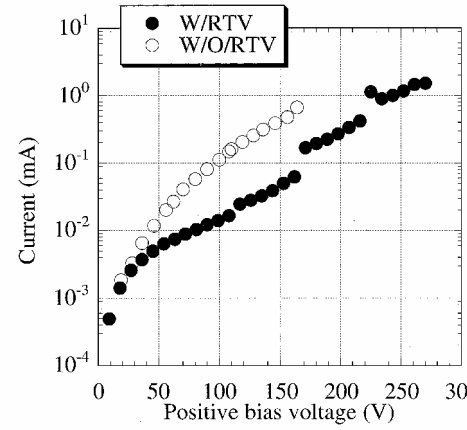

Fig. 6 Electron current collected for different positive bias values; results for W/RTV coupon (case 1) and W/O/RTV coupon (case 2). Typical error is less than 5%.

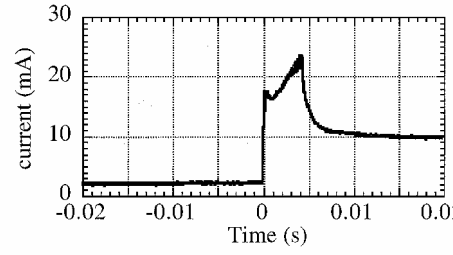

Fig. 7 Example of the current waveforms during the gas-induced glow.

biased to 310 V. The neutral density is $n_n = 0.45 \times 10^{19}$ m^{-3}, and the plasma densities is 5×10^{11} m^{-3}. Although the glow appears steady on the video, the collected current shows a pulsatile character. The collected current while the glow appears also depends on the neutral density. Therefore, the glow is due to ionization of the gas near the electron-collecting conductor. The collected current is at least three or four times larger than the current collected just before the glow inception. For an example, the maximum current collected at the neutral density of 3.2×10^{19} m^{-3} at 95 V for W/O/RTV is about 2.2 mA, whereas the maximum just before the glow inception is only 0.7 mA. For W/O/RTV, the glow is observed mostly at the bus bars, which are the largest conductors exposed to the plasma. For W/RTV, the glow is observed not only at the bus bars but also at the interconnectors because the area of the exposed bus bar was as small as the exposed interconnector in this case. In real spacecraft, a huge amount of electron current will be collected by the solar array during the glow discharge, and the power loss will be substantial. Hence, it is important to prevent the electron collection due to the snapover phenomenon, especially the gas-induced glow discharge.

Figure 8 plots the glow inception voltages for four different test coupons at various neutral gas densities. During the measurements, we increased the positive bias voltage from the lower value to the higher values in steps of 10 V at a time interval of about 1 min for each increment. Once we observed the glow on the array, the voltage was fine tuned to determine the inception voltage. We repeated the same procedure at different neutral densities. The neutral densities were increased by increasing the amount of the gas flow into the chamber. It was difficult to keep the plasma density the same for different neutral densities. Therefore, the plasma density in Fig. 8 varies for each sample, 5×10^{11}–8×10^{11} m^{-3} for W/RTV (case 1) and 1×10^{11}–3×10^{11} m^{-3} for W/O/RTV 1, 2, and 3 (case 2). From Fig. 8, note that the glow inception voltage decreases with the increase in the neutral density. The three coupons of W/O/RTV give slightly different inception voltage, which is attributed to the difference of each coupon. Nevertheless, the overall trend of W/O/RTV is the same for the three coupons. The inception voltage shows a steady decrease as the neutral density increases, and it is even lower than the operational voltage of 110 V at the extreme. On the other hand, W/RTV has a relatively constant inception voltage for the range of

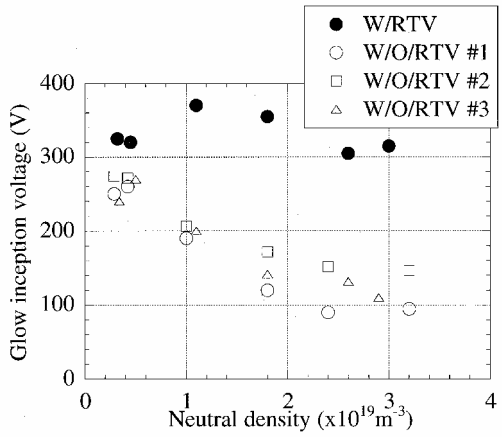

Fig. 8 Glow inception voltage at different neutral gas densities; results for four different test coupons.

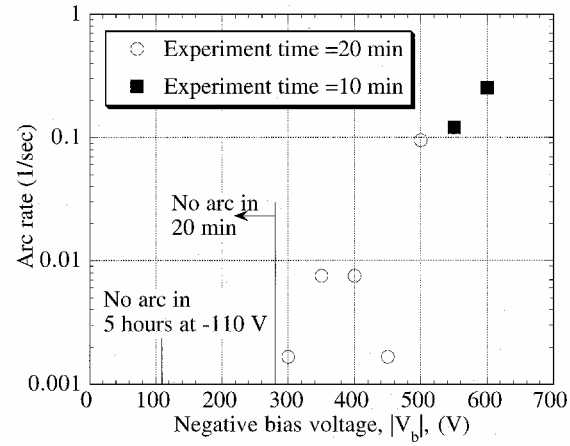

Fig. 9 Arc rate at different negative bias voltages V_b; case 3 results where W/RTV coupon is biased.

gas densities tested. It is well above the operational voltage, 110 V, even at the extreme. Therefore, covering the conductive part of the solar array with insulator, especially the bus bars, is required for solar arrays operating at a voltage higher than 100 V with ion thruster or in LEO environment. Otherwise, an accidental increase of the surrounding gas density triggers the onset of the glow discharge, which may lead to substantial loss of power and sudden drop of the spacecraft potential.

ETS-VIII has 23,056 cells, and each string (262 cells) supplies 110 V and 1.32 A of current. The total power generated by the solar array is 12.7 kW maximum. The solar array used for our experiment contains 15 solar cells. At 110 V, the collected electron current is about 0.017 mA for W/RTV and 0.16 mA for W/O/RTV, although these values might differ by several factors at different plasma and neutral densities. By extrapolating the data to 23,056 cells for the ETS-VIII case, the expected collected current for the ETS-VIII solar array that has RTV is about 26 mA at 110 V. The expected power loss of the spacecraft is about 2.8 W at its maximum. This power loss, 2.8 W, is negligible when compared to the total power generated, 12.7 kW.

Trigger Arc Inception

If the neutral density around the array increases accidentally to 10^{18}–10^{19} m^{-3}, gas-induced glow discharge might occur. If the array collects more electron current than what the neutralizer can provide, it no longer acts as a plasma contactor. The potential of the array would drop to a negative value. The maximum expected negative potential for that case is about −110 V. The ion thruster will operate for 5 h. We have biased the array at −110 V, but we have not observed any arc for 5 h. Therefore, even if a severe snapover makes the satellite potential and the array potential negative to the plasma, as long as the ion thruster beam is neutralized and the array potential is kept to −110 V at most, arcing will not occur during the normal operation of the ion thruster.

We now investigate the more severe cases, where the neutralizer fails to neutralize the ion thruster beam and the satellite potential goes down as low as −1 kV. We increased the negative bias voltage from 200 to 600 V at every 50 V. Arcs have been observed at a voltage of 300 V or more. At 250 V, no arc was observed for 20 min. Figure 9 shows the dependence of the arc rate on the negative bias voltage V_b. Generally, the arc rate increases with the bias voltage with exception of −450 V; the reason why is unknown at the present time.

Figure 10 shows the distribution of the trigger arc points on W/RTV and W/O/RTV. The trigger arc points have been identified by carrying out image processing of the video image.[12] The distribution of arc points observed on W/O/RTV is shown in Fig. 10a for a bias voltage of −700 V, $n_n = 1.8 \times 10^{19}$ m^{-3}, and $n_e = 2 \times 10^{11}$ m^{-3} (case 4). The experiment time is 20 min. Note from Fig. 10a that many arcs are observed at the interconnectors of the array, such as point a, for example. Arcs are also observed at the gap between the strings of the array, such as point b, for example. Arcs also occur at bus bars, such as point c, for example.

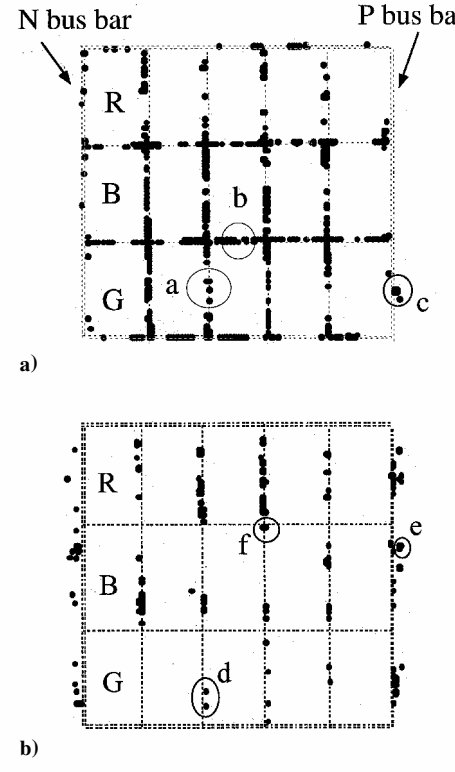

Fig. 10 Distribution of trigger arc points on a) W/O/RTV coupon at bias voltage −700 V and b) W/RTV coupon at bias voltages −500, −550, and −600 V: - - - -, cell boundaries.

Distribution of arc points on W/RTV at $n_n = 1.8 \times 10^{19}$ m^{-3} and $n_e = 7 \times 10^{11}$ m^{-3} (case 3) is shown in Fig. 10b. For this case, the results of three bias voltages, −500, −550, and −600 V, have been combined. Each bias voltage has been applied for 10 min. Many arcs are observed at the interconnectors of the array, such as point d, in Fig. 10b. Many arcs are also observed even at the bus bars, such as point e. For the case of W/RTV, bus bars are coated by RTV. However a part of N-bus bar is exposed to relax the thermal stress on the conductor. The coating at P-bus bar is not also complete, and many arcs are observed at the edge of RTV layer. Observation with an optical microscope of point e has revealed that the arc spot is located at the outer edge of RTV layer at the P-bus bar, which forms the junction with the Kapton® sheet covering the carbon fiber-reinforced plastic (CFRP) substrate. The arc probably occurred at the underlying P-bus bar through a void in the RTV. Arcs are even observed at the gap between the strings of the array that has RTV grouting, such as point f in Fig. 10b. We see a black spot left on the RTV between strings R and B. RTV grouting certainly reduces the probability of trigger arc onset. However, it is not the perfect

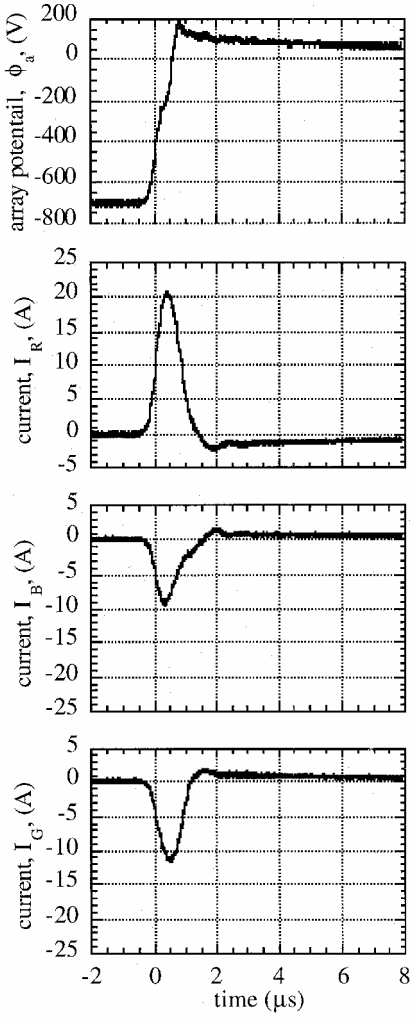

Fig. 11 Case 3 and 4 typical waveform measured examples and case 4 result.

solution unless considerable effort is spent to inspect the quality of grouting.

In Fig. 11 we show typical waveforms measured at the trigger arc inception. Figure 11 shows a result of case 4, where W/O/RTV is biased to −700 V and the neutral density is 1.8×10^{19} m^{-3}. In the example shown in Fig. 11, the trigger arc occurs at string R, where we see a positive current pulse with a peak of approximately 20 A. (See Fig. 4 for the definition of each current.) At the same time, negative current pulses flow in strings B and G, whose peak values are −9 and −11 A, respectively. The array potential ϕ_a shows a sudden increase at the arc onset because of the voltage drop across the resistance of 100 kΩ in front of the power supply. Then, the dc power supply is effectively decoupled from the arc current. The current forms loops among the strings. If we add the currents I_B and I_G, the sum becomes the mirror image of the arc current I_R. This implies that there is a current path between the arc spot and the surface of the coverglass on the nearby cells. The electrical charge flown as the arc current I_R is supplied by the coverglass and ionization along the current path. If we integrate the current I_B, the total charge that flowed from one string is 7.5×10^{-6} C, The total charge stored on the coverglass of one string ($C_g = 3.5$ nF per string) is estimated to be about 2.5×10^{-6} C. Therefore, the additional ionization provides 5.0×10^{-6} C. The charge provided from the other nonarced string increases due to ionization as the gas density increases. The effect, however, is much smaller than the effect of a dc power supply inserted directly between the strings, as it is shown later in discussion of the sustained arc formation.

In Fig. 12, we show the temporal profile of the arc count at different neutral gas densities measured in case 4. In Fig. 12, the gas densities are denoted per cubic meter. The number of arcs has been counted via image processing of the video image taken

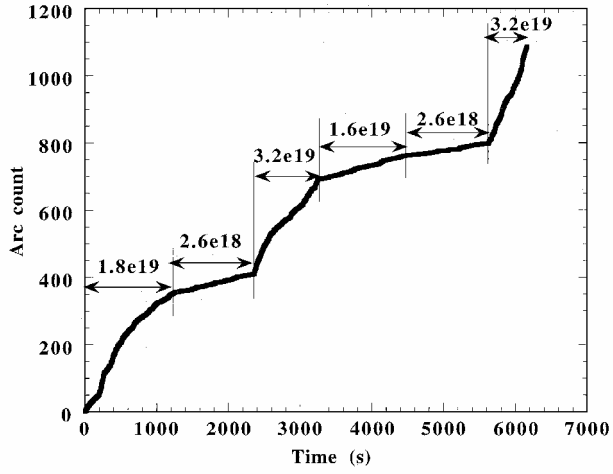

Fig. 12 Temporal profile of arc count during experiment where neutral gas density is varied in time; case 4 results.

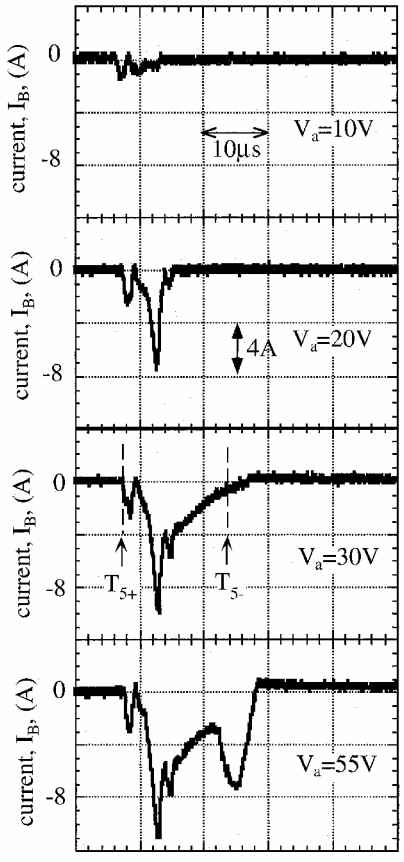

Fig. 13 Example of typical waveforms of the current flowing to string B, I_B, when arcs occur at string R for different interstring bias voltage V_a; case 5 results.

during the experiment. The plasma density also varies as the gas density changes, from $n_e = 3 \times 10^{11}$ m^{-3} for $n_n = 3.2 \times 10^{19}$ m^{-3} to $n_e = 1 \times 10^{11}$ m^{-3} for $n_n = 2.6 \times 10^{18}$ m^{-3}. The experiment time at each gas density is about 20 min except $n_n = 3.2 \times 10^{19}$ m^{-3}. In Fig. 12, the steeper the gradient gets, the more frequent arcs occur. Because arcs tend to occur less and less as time goes on even at the same experimental condition, so-called conditioning effect, we first lowered the density and and raised again. Even taking into account the conditioning effect, Fig. 12 shows more arcs at higher gas density.

Sustained Arc

In the present investigation, we use the negative bias voltage of −500 or −700 V to simulate the drop of array potential to −1 kV due to the failure of neutralizer because, if we had biased to −1 kV, too many arcs would occur and disturb the measurement. In Fig. 13,

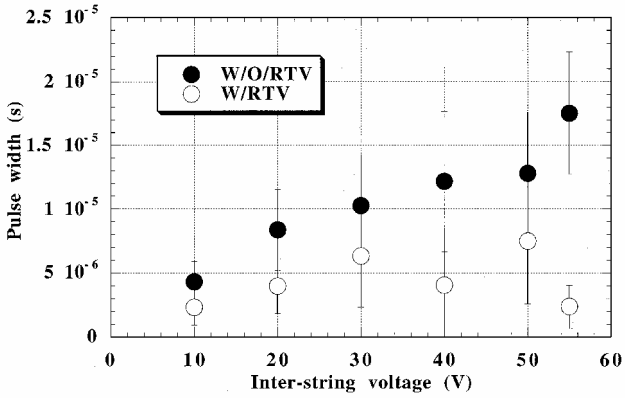

Fig. 14 Pulse width of neutralization current flow to string B when a trigger arc occurs at string R for different interstring bias voltages; case 5 and 6 results.

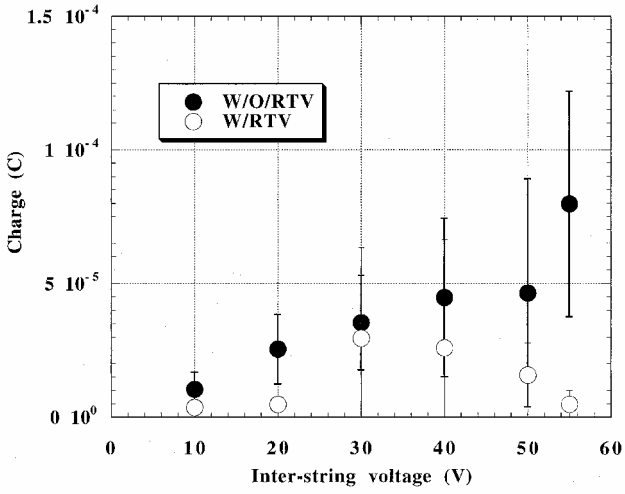

Fig. 15 Charge flow to string B as the neutralization current when a trigger arc occurs at string R for different interstring bias voltages; case 5 and 6 results.

typical waveforms measured in case 5 at various interstring voltages V_a are shown. In Fig. 13, we show the current flowing to string B, I_B, when arcs occur at string R. These are the neutralization currents feeding the energy to the trigger arc plasma.[13] Once an arc occurs at string R, a positive current (discharge current) flows, as shown in Fig. 11. The energy for the discharge current is supplied by the charges stored in the coverglass of strings B and G as shown in Fig. 11. In Fig. 13, T_{5+} is the time when the current has 5% of the peak of the neutralization current I_B for the first time. The time T_{5-} is the time when the current becomes 5% of the peak of the neutralization current for the last time. The pulse width is defined as the time difference between T_{5-} and T_{5+}. In Fig. 14, we plot the pulse width of the neutralization current at different interstring bias voltages V_a between strings R and B for W/RTV and W/O/RTV at the neutral density of 2.2×10^{19} m^{-3} and at the plasma density of 1×10^{11}–2×10^{11} m^{-3}. The error bars indicate the standard deviation. Each point is an average of at least 3 measurements and a maximum of 24 measurements. From Fig. 14, it is seen that the pulse width is smaller for the case of W/RTV. The pulse width increases with the increase in the interstring voltage for both the cases.

Figure 15 shows the charge released from string B at different values of the interstring voltage between strings R and B. It is calculated by integrating I_B with respect to time. Each point is an average of at least 3 measurements and a maximum of 24 measurements. The released charge increases with the increase in the interstring voltage V_a, but the charge is higher for solar arrays W/O/RTV. Note that the coverglass of string B can supply only 1.7×10^{-6} C to the arc. Even if ionization is taken into account, it is more or less 1.0×10^{-5} C as discussed with Fig. 11. The fact that a charge far greater than those values is supplied by string B to the arc indicates that the power supply between the strings R and B contributes the additional charge to the arc plasma. As long as the pulse width and the amount of charge are limited to finite values, the trigger arc ends as single pulses. However, when the pulse width becomes infinite, it means that the power supply keeps supplying the current between the strings.

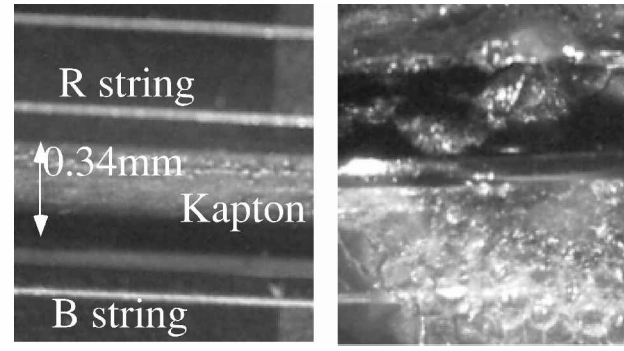

Before experiment **After experiment**

Fig. 16 Microscope photograph of sustained arc site on W/O/RTV coupon, taken after case 5 experiment.

For W/O/RTV, we observed the sustained arc between strings R and B at the plasma and neutral densities of 3×10^{11} and 2.2×10^{19} m^{-3}. Before this plasma density, we had increased the interstring bias voltage V_a from 10 to 55 V with the plasma density of 1×10^{11}–2×10^{11} m^{-3}. Each bias had been applied for 20 min. Because we did not observe the sustained arc at $V_a = 55$ V, we increased the plasma density to 3×10^{11} m^{-3} to make more arcs occur. Then in 2 min we observed a sustained arc. Therefore, if we had waited long enough, a sustained arc would have occurred even at 2×10^{11} m^{-3}. Otherwise, the slight change of the ambient plasma density determines whether the sustained arc occurs, which is hard to justify. When the sustained arc occurred, the bias voltage ($V_a = 55$ V) dropped to 7 V and the current indicator showed the preset maximum current of $I_{\max} = 2.64$ A. We switched off the array bias ($V_b = -500$ V), yet the current kept flowing for more than 10 s, until we finally switched off the interstring bias. Microscope photographs of the sustained arc point between strings R and B is given in Fig. 16. From the photographs, it is seen that the sustained arc damaged the strings and Kapton film (50 μm) on a CFRP face sheet (0.1 mm) substrate on which the cells were mounted. The inspection after the experiment revealed that the two strings and substrate were completely short circuited.

The model for the sustained arc formation between the adjacent cells of W/O/RTV is given in Fig. 17. When there is no RTV grouting between adjacent solar cell strings, trigger arcs may occur at the point where the triple junction is formed by adhesive, solar cell, and plasma. The arc plasma grows by receiving the energy from the external capacitance. This current path is shown as the broken line in Fig. 17a. Then a dense arc plasma is produced at the arc spot, which makes a direct coupling with the nearby exposed conductor (cell electrode) of the adjacent cell. Then the direct short circuit between the strings is developed, and the arc is sustained by the power supply V_a. This current path is shown as the solid line in Fig. 17a. As the current keeps flowing through the arc plasma, the underlying Kapton sheet finally breaks down, and there is short circuit between the solar cell strings and the underlying conductive substrate. Then the permanent short circuit occurs between the string, and the current continues as long as the power supply works. This current path is shown in Fig. 17b.

In the ETS-VIII solar array there are 88 strings (2 wings). Each string has a capacitance of 180 nF. One wing of the solar array has a total of 8-μF capacitance. In the case of failure of the neutralizer, the potential of the spacecraft body may reach up to -1 kV. The power supply of the ion thruster has the function to detect the failure of the neutralizer. When the failure occurs, the beam voltage will be shut down within several milliseconds. In this small time gap, a potential difference of about 300 V will develop between the coverglass and the interconnector, considering the ion thermal flux derived from the density near the solar array. At this potential difference, one wing of the array can supply energy $E = \frac{1}{2} \times (8 \times 10^{-6}) \times (300)^2 = 0.36$ J to the arc.

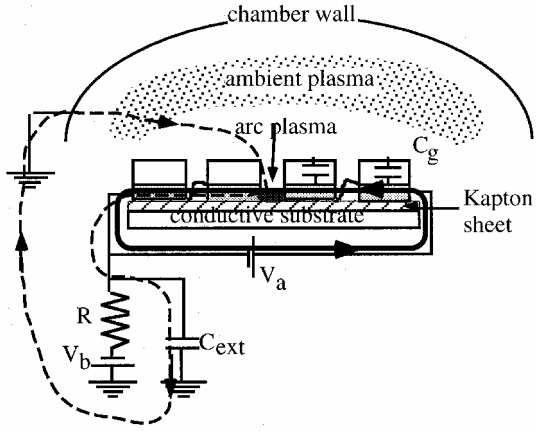

a) Trigger arc inception and sustained arc formation

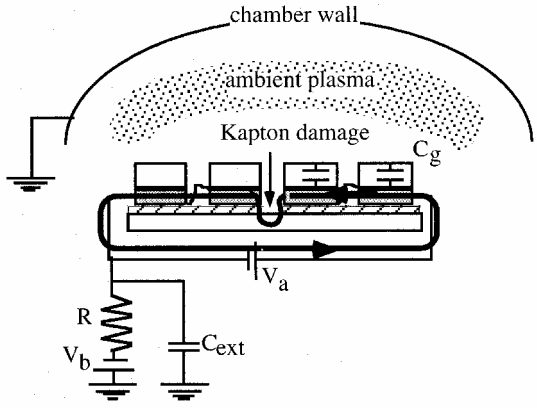

b) Short-circuit through conductive substrate

Fig. 17 Schematic of sustained arc formation for W/O/RTV coupon in laboratory experiment.

In case 7, we inserted additional capacitance in the external circuit and examine whether the described condition leads to a sustained arc or not in the case of W/RTV. We increased the capacitance from 180 to 1440 nF in steps of 180 nF at the bias voltage of −500 or −700 V with the interstring potential difference of 55 V and current capability of 2.64 A. We simulated the worst condition in our experiments by inserting the capacitance of $C_{ext} = 1440$ nF at the bias voltage of $V_b = -700$ V, so that it would deliver the energy of 0.36 J to an arc. A test coupon was biased for at least 10 min for each condition, and the worst condition, ($V_b = -700$ V and $C_{ext} = 1440$ nF) was tested for 80 min. Although more than 100 trigger arcs occurred under the worst condition, a sustained arc did not occur. This result verifies that even if the neutralizer stops operating in orbit and one wing of the solar array supplies energy to the arc, a sustained arc will not occur between the solar cell strings with RTV grouting.

We increased the interstring bias voltage V_a from 60 V at a step of 10 V, until we see a sustained arc on W/RTV while fixing all of the other parameters. Each interstring bias voltage V_a was applied for 20 min. At each bias voltage, at least 20 trigger arcs were observed. As the voltage V_a increased beyond 100 V, we observed very bright flash at more than two points over the array. One of the flashes always occurred on string R and the other points are on string B or G. This observation suggested that a trigger arc on string R found connection points on the other strings. Occasionally, we observed that the interstring bias power supply showed a brief transition to the constant current mode, indicating that the power supply provided the current for a short period. The multiple flashes, however, did not continue more than two video frames (66 ms). Finally, at $V_a = 130$ V, we observed a sustained arc, as shown in Fig. 18. The sustained arc occurred between an interconnector on string R and an interconnector on string B separated by 6 cm. Observation by an optical microscope revealed that the interconnector at string R was completely blown off. The interconnector at string B was not only blown off, but also suffered significant melting. The bright flash

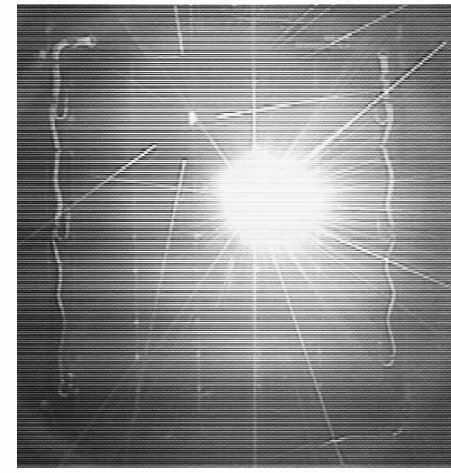

Fig. 18 Video image of sustained arc between strings R and B on W/RTV coupon; case 8 result, where interstring bias voltage 130 V is applied.

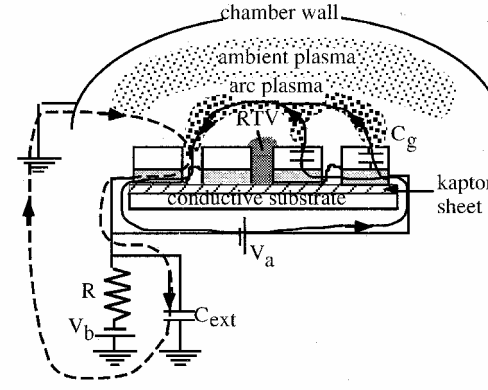

a) Trigger arc inception and arc plasma growth

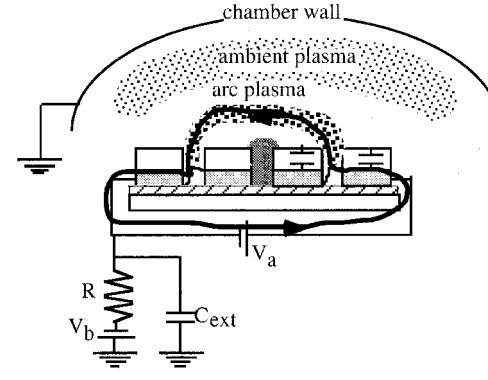

b) Sustained ac formation

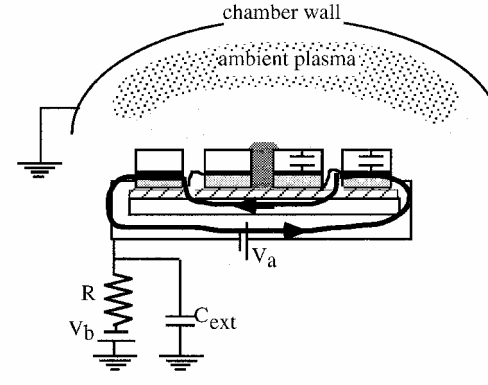

c) Short-circuit through conductive substrate

Fig. 19 Schematic of sustained arc formation for W/RTV coupon in laboratory experiment.

shown in Fig. 18 continued for eight video frames and vanished after that, though the current of 2.64 A kept flowing at the voltage drop of $V_a = 10$ V even after we switched off the array bias ($V_b = -700$ V). Inspection after the experiment revealed that strings R and B were both short circuited to the substrate. Therefore, after eight video frames, the current flew through the substrate.

If enough energy is given to the arc plasma, a sustained arc can occur in a form bridging remotely located conductive areas via the arc plasma. We show such a model in Fig. 19. Once a trigger arc occurs at an interconnector, the arc current flows through the capacitance connected in the external circuit to the chamber wall and closes the current path. This is the same as the case of W/O/RTV and is shown as the broken line in Fig. 19a. As the arc plasma grows, it extends further and couples with the coverglass of the nearby solar cells. The coverglass acts as another capacitance C_g because it stores charges before the trigger arc inception and supplies the energy to the arc plasma. This current path is shown as the solid line in Fig. 19a. As the arc plasma grows, it finds an exposed interconnector of the adjacent string. If the conductivity of the arc plasma is high enough, it can carry the current supplied by the power supply V_a. This current path is shown in Fig. 19b and also corresponds to the video image in Fig. 18. As the current keeps flowing, the excessive heating at the arc spot and its counterpart causes the underlying Kapton sheet to break down. Then the permanent short circuit occurs between the two strings and the short-circuit current keeps flowing through the underlying conductive substrate. This current path is shown in Fig. 19c.

Conclusions

Because of the operation of ion thrusters for north–south station keeping, even a GEO satellite is surrounded by a plasma whose density is comparable to LEO environment. Laboratory experiments have been carried out to study the interaction between the ion thruster plasma and the solar arrays of the ETS-VIII satellite. The results of the electron current measurements for two different designs of solar arrays that are planned to operate at 110 V shows that the solar array with RTV grouting between the cells and on the bus bars (W/RTV) collects much less electron current compared to the W/O/RTV solar array. The threshold voltage for the gas-induced glow discharge is lower for the case of W/O/RTV, even lower than 100 V at the extreme case. However, the gas-induced glow does not occur for W/RTV at 110 V even at the worst case of neutral density increase mainly because the bus bar is coated by RTV, hiding a large area of the positively biased conductor from the plasma. The power loss of the spacecraft will be negligible compared to the total power of the satellite as long as RTV grouting is used.

The potential drop of the solar array due to the anomalous electron collection to the solar array has been simulated, but we have not observed any arc at a bias voltage of -110 V for 5 h. The arc rate has strong dependence on the bias voltage and the neutral density. The failure of the ion thruster neutralizer has been simulated, and we have observed a sustained arc between the adjacent cells of W/O/RTV at a voltage of 55 V and maximum current of 2.64 A. The sustained arc short circuited between the two strings of the array and led to destruction of the solar array circuit. The RTV grouting between the adjacent cells has prevented sustained arc formation under the operational condition of the ETS-VIII. We have inserted additional capacitance in the test system, but we have not observed a sustained arc between the strings even under the worst condition, where the ion thruster neutralizer fails and one entire wing of the solar array coverglass supplies the energy to the trigger arc. Increase in the interstring voltage in the solar array with RTV to $V_a = 130$ V at maximum current $I_{\max} = 2.64A$ at a bias voltage of $V_b = -700$ V finally led to a sustained arc formation between two interconnectors separated by 6 cm. This threshold gives a sufficient safety margin to the present design of the ETS-VIII array for flight use employing RTV grouting.

The use of RTV around the cells and the bus bar coatings is considered as the minimum requirement for the spacecraft with an HV bus system such as the ETS-VIII. We suggest the following mitigation strategies: 1) Prevent the increase of the gas density around the solar array to further reduce the possibility of glow discharge inception and trigger arcs. 2) Put the block diode at the positive end of the array circuit to protect the other strings from the short circuit with the substrate even if one string is lost due to a sustained arc.

Acknowledgments

The authors thank the members of Toshiba Corp., Japan, for the array sample fabrication. The authors greatly acknowledge M. Hikita of Kyushu Institute of Technology (KIT), H. Kuninaka of the Institute of Space and Aeronautical Science (ISAS), H. Nishimoto of the National Space Development Agency for discussions, and Y. Ozaki of Mitsubishi Electric Corp. for the plasma diagnostics of the ion thruster plume. The authors also thank S. Sasaki and K. Tanaka of ISAS for lending a plasma source. The authors extend their thanks to the students of KIT, J. Arai, T. Matsumoto, H. Fukushima, and K. Matsura, for their help with the experiment.

References

[1] Hastings, D. E., and Garrett, H., *Spacecraft-Environmental Interactions*, Cambridge Univ. Press, New York, 1996, Chap. 5.

[2] Hastings, D. E., and Chang. P., "The Physics of Positively Biased Conductors Surrounded by Dielectrics in Contact with Plasma," *Physics of Fluids B*, Vol. 1, No. 2, 1989, pp. 1123–1132.

[3] Galofaro, J. T., Ferguson, D. C., Vayner, B. V., Degroot, W. A., Thomson, C. D., Dennison, J. R., and Davies, R. E., "Inception of Snapover and Gas Induced Glow Discharges," AIAA Paper 2000-0245, Jan. 2000.

[4] Cooke, D. L., and Katz, I., "Ionization-Induced Instability in an Electron Collecting Sheath," *Journal of Spacecraft and Rockets*, Vol. 25, No. 2, 1988, pp. 132–138.

[5] Cho, M., "Ionosphere Ionization Effects on Sheath Structure Around a High-Voltage Spacecraft," *Journal of Spacecraft and Rockets*, Vol. 32, No. 6, 1995, pp. 1018–1026.

[6] Cho, M., "Ionization Around a High-Voltage Body in Magnetized Nonflowing Ionospheric Plasma," *Journal of Spacecraft and Rockets*, Vol. 35, No. 1, 1998, pp. 90–99.

[7] Hastings, D. E., Cho, M., and Kuninaka, H., "The Arcing Rate for a High Voltage Solar Array: Theory, Experiment and Predictions," *Journal of Spacecraft and Rockets*, Vol. 29, No. 4, 1992, pp. 538–554.

[8] Katz, I., Davis, V. A., and Snyder, D. B., "Mechanism for Spacecraft Charging Initiated Destruction of Solar Arrays in GEO," AIAA Paper 98-1002, Jan. 1998.

[9] Cho, M., Ramsamy, R., Matsumoto, T., Toyoda, K., Nozaki, Y., and Takahashi, M., "Laboratory Tests on 110-Volt Solar Arrays in a Simulated Geosynchronous Orbit Environment," *Journal of Spacecraft and Rockets*, Vol. 40, No. 2, 2003, pp. 211–220.

[10] Davis, S., Stillwell, R., Andiario, W., Snyder, D., and Katz, I., "EOS-AM Solar Array Arc Mitigation Design," Society of Automotive Engineers, 34th Intersociety Energy Conversion Engineering Conf., SAE TP 1999-01-2582, Aug. 1999.

[11] Takahashi, M., Nishimoto, H., Cho, M., Nozaki, Y., Fujii, H., Murakami, Y., Ozaki, T., and Onodera, N., "ETS-VIII Solar PDL Plasma Interaction Problem Approach," *Proceedings of 7th Spacecraft Charging Technology Conference*, ESA, Noordwijk, The Netherlands, 2001, pp. 127–132.

[12] Shiraishi, K., Cho, M., and Hikita, M., "Optical Measurement of Charging and Discharging Processes on Insulator Surface in Simulated Low Earth Orbit Plasma Environment," *Proceedings of 26th International Electric Propulsion Conference*, JSASS, Kitakyushu, Japan, 1999, pp. 1351–1355.

[13] Cho, M., Ramasamy, R., Hikita, M., Tanaka, K., and Sasaki, S., "Plasma Response to Arcing in LEO Plasma Environment: Laboratory Experiment," *Journal of Spacecraft and Rockets*, Vol. 39, No. 3, 2002, pp. 392–399.

D. L. Edwards
Associate Editor